New Phytologist

Research

Ligand-induced ubiquitination regulates endocytosis and homeostasis of the ERECTA receptor kinase for stomatal development

Liangliang Chen[1,2]*, Minh Huy Vu[1,2]*, Pengfei Bai[1,2], Alicia M. Cochran[1,2], Crystal F. Ying[2] and Keiko U. Torii[1,2]

[1]Howard Hughes Medical Institute, The University of Texas at Austin, Austin, TX 78712, USA; [2]Department of Molecular Biosciences, The University of Texas at Austin, Austin, TX 78712, USA

Author for correspondence:
Keiko U. Torii
E-mail: ktorii@utexas.edu

Received: *15 February 2026*
Accepted: *9 March 2026*

New Phytologist (2026) **250:** 3167–3181
doi: 10.1111/nph.71151

Key words: endocytosis, inflorescence/pedicel elongation, peptide hormone, receptor kinase, stomatal development, ubiquitination.

Summary

• Stomatal patterning on the plant epidermis is regulated by the ERECTA family of leucine-rich repeat receptor kinases (LRR-RKs). While ubiquitination has emerged as a key regulatory mechanism for the endocytosis of receptor kinases, the precise molecular connections among ERECTA ubiquitination, endocytosis, and its biological functions remain unclear. Here, we uncover a critical role of ligand-induced ubiquitination in regulating the endocytosis and homeostasis of the ERECTA receptor kinase for stomatal development and elongation of inflorescence pedicels in *Arabidopsis thaliana*.

• Previous ubiquitome profiling of plant membrane proteins identified one ubiquitination site in ERECTA, and our sequence alignment analysis identified two additional ubiquitination sites within the juxtamembrane domain. We subsequently performed site-directed mutagenesis of these lysine residues (K617, K625, and K668) to arginine ($ERECTA_{3KR}$). Our phenotypic analyses demonstrate that the mutant version of ERECTA confers over-inhibition of stomatal development and excessive pedicel growth, indicating that the absence of ubiquitination confers hyperactivity of ERECTA. Our biochemical analyses further demonstrate that the perception of EPIDERMAL PATTERNING FACTOR2 (EPF2) peptide ligand induces K63-linked ubiquitination of ERECTA mediated by PUB30 and PUB31. By contrast, the ligand-induced K63-linked polyubiquitination is impaired in $ERECTA_{3KR}$.

• K63-ubiquitin chains are considered to be a general signal for endocytosis for plasma membrane proteins. Notably, impaired K63-linked ubiquitination of ERECTA compromises its ligand-induced endocytosis, as well as subsequent trafficking to multivesicular bodies and the vacuole for degradation. Moreover, $ERECTA_{3KR}$ exhibits reduced co-localization with endocytic trafficking markers (ARA6 and SYP43). Consistently, $ERECTA_{3KR}$ accumulates to a higher protein level than wild-type ERECTA and exhibits reduced sensitivity to ligand application, as well as pharmacological inhibition of clathrin-mediated endocytosis or vacuolar degradation.

• Together, our findings reveal that K63-linked ubiquitination of ERECTA is essential for its ligand-induced endocytosis and vacuolar degradation, thereby ensuring proper signal attenuation. The absence of this post-translational modification leads to sustained plasma membrane accumulation of active receptors, resulting in excessive inhibition of stomatal development. Therefore, our study highlights that ERECTA signals at the plasma membrane and that ubiquitination serves as a key mechanism for fine-tuning receptor kinase activity and developmental outcomes in plants.

Introduction

Precise regulation of stomatal patterning optimizes plant gas exchange and water-use efficiency (Pillitteri & Torii, 2012). In *Arabidopsis thaliana*, this process is tightly controlled by cell–cell signaling mediated by receptor-like kinases (RLKs; those with known ligands are referred hereafter as receptor kinases (RKs)). Among them, the ERECTA family plays a central role. ERECTA, together with its paralogs ERL1 and ERL2, negatively regulates stomatal formation by perceiving a family of secreted peptide ligands, EPIDERMAL PATTERNING FACTORs (EPFs) and EPF-LIKEs (Hara *et al.*, 2007, 2009; Hunt &

*These authors contributed equally to this work.

© 2026 The Author(s).
New Phytologist © 2026 New Phytologist Foundation.
This is an open access article under the terms of the Creative Commons Attribution License, which permits use, distribution and reproduction in any medium, provided the original work is properly cited.

Gray, 2009; Kondo *et al.*, 2010; Sugano *et al.*, 2010). Among the ERECTA-family members, ERECTA is expressed in protodermal- and early stomatal-lineage cells. ERECTA primarily perceives EPF2 and activates a downstream mitogen-activated protein kinase (MAPK) signaling cascade, leading to the inhibition of the master transcription factors of stomatal development (Lampard *et al.*, 2008; Lee *et al.*, 2012; Horst *et al.*, 2015). Consequently, loss-of-function mutations in *ERECTA* result in excessive asymmetric cell divisions, thereby increasing the number of stomatal precursor cells, meristemoids (Shpak *et al.*, 2005; Lee *et al.*, 2012). In addition to its role in stomatal patterning, ERECTA regulates aerial organ growth, notably inflorescence and pedicel elongation (Torii *et al.*, 1996; Shpak *et al.*, 2004; Shpak, 2013). Here, ERECTA expressed in the internal tissue perceives EPFL4/6 to promote cell proliferation in a non-cell autonomous manner (Uchida *et al.*, 2012). While the downstream signaling pathway for ERECTA-mediated stem/pedicel elongation is less established, it also mediates the MAPK cascade (Meng *et al.*, 2012).

Studies over the past decade revealed the mechanism of ERECTA receptor activation (Bai & Torii, 2026). ERECTA constitutively forms a receptor complex with TOO MANY MOUTHS (TMM) (Nadeau & Sack, 2002; Lee *et al.*, 2012, 2015). Before ligand perception, the activity of ERECTA is inhibited by BRI1-KINASE INHIBITOR1 (BKI1) (Wang *et al.*, 2017; Chen *et al.*, 2025). Perception of EPF2 peptides recruits co-receptors SOMATIC EMBRYOGENESIS RECEPTOR KINASE1 (SERK1), SERK2, and BRI1-ASSOCIATED KINASE (BAK1)/SERK3 (Lee *et al.*, 2012, 2015; Meng *et al.*, 2012, 2015; Lin *et al.*, 2017). BAK1 subsequently transphosphorylates the C-terminal tail domain of ERECTA. This triggers eviction of BKI1 from ERECTA and recruitment of ubiquitin E3 ligases, PLANT U-BOX 30 (PUB30) and PUB31, which in turn downregulate the activated ERECTA (Chen *et al.*, 2023, 2025). This intricate mechanism of ERECTA attenuation also operates during inflorescence/pedicel elongation. Consistently, loss-of-function *pub30 pub31* double mutant plants exhibit a greatly reduced number of stomata and extremely elongated inflorescence and pedicels due to excessive accumulation of ERECTA proteins (Chen *et al.*, 2023).

Protein ubiquitination (also known as ubiquitylation) is an important post-translational modification, and the type of ubiquitination, such as mono- vs polyubiquitination as well as the linkage type dictates the stability, activity, and/or subcellular dynamics of target client proteins (Leitner *et al.*, 2012; Dubeaux *et al.*, 2018; Romero-Barrios & Vert, 2018). For instance, lysine 48 (K48)-linked polyubiquitination marks target proteins for proteasomal degradation, including degradation of some membrane proteins in mammals (Foot *et al.*, 2017). In plants, K63-linked polyubiquitination has emerged as a key mechanism for membrane protein degradation through impacting their subcellular localizations (Romero-Barrios & Vert, 2018; Hasegawa *et al.*, 2024). For example, K63 polyubiquitination of the brassinosteroid hormone receptor BRI1 promotes its internalization and vacuolar degradation via multivesicular bodies (MVBs), providing an important means of fine-tuning the duration of receptor signaling (Martins *et al.*, 2015; Zhou *et al.*, 2018). As mentioned above, we have previously identified PUB30 and PUB31 as the E3 ubiquitin ligases that mediate the ubiquitination of ERECTA in response to peptide ligand stimulation (Chen *et al.*, 2023, 2025). However, the exact sites or types of polyubiquitination as well as the mechanistic consequences of ERECTA ubiquitination on its intracellular trafficking remain largely unexplored.

In this study, we investigated the functional significance of ERECTA ubiquitination for its protein behaviors and phenotypic consequences. For this purpose, we surveyed publicly available ubiquitome data as well as inference from the studies of other plant RKs and generated ubiquitination-deficient ERECTA variants, in which three lysine residues (K617, K625, and K668) were substituted by arginine. We examined the effects of this mutant receptor on stomatal development, ubiquitination, intracellular trafficking of ERECTA, and the receptor protein abundance. Our results demonstrate that K63-linked ubiquitination of ERECTA is essential for its ligand-induced endocytosis and eventual vacuolar degradation. Mutagenesis of these three residues results in reduced endocytosis of ERECTA, increased receptor abundance, and a hyperactive inhibition of stomatal development. These findings uncover a critical role for ubiquitination in constraining ERECTA signaling output and provide mechanistic insight into how post-translational regulation governs receptor function during plant development.

Materials and Methods

Plant materials and growth conditions

The *Arabidopsis thaliana* (L.) Heynh accession Columbia (Col-0) was used as the wild-type. All plants used in this study are in a Col background. The following mutants and transgenic plant lines were previously reported: *er-105*; *pub30 pub31*; *ERECTApro::gERECTA-FLAG* in *er-105* (Chen *et al.*, 2025). *ubc35 ubc36* is a gift from Prof. Marco Trujillo's lab. Arabidopsis seeds were surface sterilized with 30% bleach and grown on half-strength Murashige and Skoog media containing 1× Gamborg Vitamin (Sigma), 0.75% Bacto Agar and 1% w/v sucrose for 9 d and then transplanted into soil. Plants were grown under long-day conditions (16 h : 8 h, light : dark) at 22°C.

Plasmid construction and generation of transgenic plants

For recombinant protein expression, the following plasmids were previously reported: pJA51 (MBP-ERECTA_CD), pCLL107 (GST-PUB30), and pCLL109 (GST-PUB31) (Chen *et al.*, 2023, 2025). The following plasmids were generated: pCLL194 (MBP-ERECTA_CD$_{K617RK668R}$, MBP-ERECTA_CD$_{2KR617}$), pCLL193 (MBP-ERECTA_CD$_{K625RK668R}$, MBP-ERECTA_CD$_{2KR625}$), and pCLL285 (MBP-ERECTA_CD$_{K617RK625RK668R}$, MBP-ERECTA_CD$_{3KR}$). Site-directed mutagenesis was performed using a PCR overlap extension followed by assembly into linearized vector pMALC2. For complementation assays, the following plasmids were generated: pCLL284 (*ERECTApro::gERECTA*$_{K668R}$-

© 2026 The Author(s).
New Phytologist © 2026 New Phytologist Foundation.

FLAG), pCLL200 (*ERECTApro::gERECTA$_{K625RK668R}$-FLAG*), pCLL201 (*ERECTApro::gERECTA$_{K617RK668R}$-FLAG*), pCLL287 (*ERECTApro::gERECTA$_{K617RK625RK668R}$-FLAG*), pCLL283 (*ERECTApro::gERECTA-YFP*), and pCLL288 (*ERECTApro::gERECTA$_{K617RK625RK668R}$-YFP*). A three-way Gateway system was utilized to generate a series of ERECTA constructs driven by the ERECTA promoter. See Supporting Information Tables S1 and S2 for details of plasmid and oligo DNA information. Plasmids were transformed into Agrobacterium GV3101/pMP90 and subsequently into Arabidopsis by floral dipping. Over 10 lines were characterized for the phenotypes and reporter gene expressions.

Microscopy for stomatal phenotype

Confocal microscope images for stomatal phenotype were taken as previously described using Leica SP5-WLL operated by LAS AF (Leica Microsystems, Deerfield, IL, USA). Cell peripheries of seedlings were visualized with propidium iodide (Molecular Probes, Thermo Fisher Scientific, Waltham, MA, USA). Fluorescence signals were detected under the following conditions: Propidium iodide, excitation at 561 nm and the emission range from 582 to 617 nm. For internalization imaging of ERECTA-YFP, ERECTA$_{3KR}$-YFP and other membrane organelle markers, Z-stack images were acquired at 0.49 μm intervals to cover the entire epidermal cell depth at a resolution of 1024 × 1024 pixels. Maximum intensity projections were generated using Leica LAS AF software and analyzed with Fiji (https://imagej.net). Images were captured using either a 20× water-immersion objective for stomatal observation or a 63× water-immersion objective for endocytosis assays. Fluorescence signals were detected under the following conditions: YFP, excitation 514 nm and emission range from 518 to 550 nm; RFP and FM4-64, excitation 555 nm and emission range from 573 to 630 nm. For endosome-labeled FM4-64 quantification, the maximum projection of Z-stack images was then generated by Leica LAS AF software. For Wortmannin treatment, seedlings were incubated with 30 μM Wortmannin (in 0.25% DMSO) for 90 min with gentle shaking. A mock control consisted of 0.25% DMSO in half-strength MS liquid. For mEPF2 treatment, the purified peptide solution was diluted to 5 μM using half-strength MS liquid and incubated with seedlings for 90 min under gentle shaking. For Con A treatment, seedlings were treated with 1 μM Con A (ab144227; Abcam, Cambridge, UK) in water for 6 h. All the treatments were pre-stained with 8 μM of FM4-64 for 10 min. Endosomes were defined as structures with diameters of 0.2–0.5 μm, while Wm bodies were defined as punctae larger than 0.5 μm (Qi *et al.*, 2020). Each experiment was repeated at least three times, each with at least three seedlings per repeat. The confocal images were false colored, and brightness/contrast were uniformly adjusted using Photoshop 2022 (Adobe, San Jose, CA, USA).

Quantitative analysis and statistics

For analysis of the epidermis, abaxial cotyledons from 7-d-old seedlings of relevant genotypes were subjected to PI staining and confocal microscopy. The central regions overlying the distal vascular loop were imaged, and the number of epidermal cells, stomata, and meristemoids was quantified. Pedicel lengths were measured using ImageJ. Statistical analysis was performed using R v.4.4.0 operated under R-Studio v.2025.05.0+496 (https://www.rstudio.com), and graphs were generated using R ggplot2 package. For all violin plots, the shape of each violin represents the kernel density estimation of the data distribution across its range, with the width at each vertical position corresponding to the local data density. Each dot represents a jittered individual data point. For genotype–phenotype comparison, one-way ANOVA followed by Tukey's HSD test was performed for comparisons among multiple groups. Statistical differences were indicated by different letters (e.g. a, b, c, d) at a threshold of *P*-value ($P < 0.05$). For individual sample size (n), see corresponding figures or figure legends. The original quantitative data are provided as Dataset S1.

Gene expression levels in RT-qPCR analysis, quantification of endosomes, and protein abundance from immunoblot assays were analyzed using GraphPad Prism software (v.10.3.0 (461), GraphPad Software). For comparisons between matched samples, Welch's unpaired *t*-tests were performed. For individual sample size (n) and *P*-values, see corresponding figures or figure legends.

Expression, purification, and refolding of peptides

Recombinant mEPFL6 peptide was prepared as described previously (Lee *et al.*, 2012). Bioactivities of the refolded mEPFL6 peptide were confirmed as described previously (Lee *et al.*, 2012).

In vitro and *in vivo* ubiquitination assays

The *in vitro* ubiquitination reactions contained 1 μg each of substrate (MBP-ERECTA_CD, MBP-ERECTA_CD$_{2KR617}$, ERECTA_CD$_{2KR625}$ or MBP-ERECTA_CD$_{3KR}$), HIS-E1 (AtUBA1), HIS-E2 (AtUBC8 or AtUBC35), HIS-ubiquitin (Boston Biochem, Cambridge, MA, USA) and GST-PUB30 in the ubiquitination reaction buffer (0.1 M Tris–HCl, pH 7.5, 25 mM $MgCl_2$, 2.5 mM dithiothreitol and 10 mM ATP; the final volume 30 μl). The reactions were incubated at 30°C for 3 h, stopped by adding 4× SDS sample loading buffer and boiled at 95°C for 5 min. The samples were then separated by 8% SDS–PAGE, and the ubiquitinated ERECTA_CDs were detected by immunoblot analysis with anti-MBP (E8032, 1 : 10 000; New England Biolabs, Ipswich, MA, USA) as the primary antibody, whereas the auto-ubiquitination was detected by immunoblot analysis with anti-GST (ab92, 1 : 5000; Abcam) as the primary antibody. As a secondary antibody, goat anti-mouse IgG H&L (HRP) (ab205719; Abcam) was used at a dilution of 1 : 5000. The protein blots were visualized using a Chemi-luminescence assay kit (34095; Thermo Fisher Scientific, Waltham, MA, USA) and the Image Lab software (v.6.0.1; Bio-Rad).

For *in vivo* ubiquitination assays, fresh Arabidopsis protoplasts were co-transfected with FLAG-tagged ubiquitin (FLAG-UBQ), HA-tagged ERECTA variants, together with a control vector or MYC-tagged PUB30, and incubated for 9 h followed by treatment with 5 μM mEPFL6 for 1 h in the presence of protease inhibitor MG132 (5 μM; M7449; Sigma). The ubiquitinated

© 2026 The Author(s).
New Phytologist © 2026 New Phytologist Foundation.

ERECTA variants were detected with α-HA (ab18181, 1 : 1000; Abcam) and anti-Ubiquitin (linkage-specific K63) antibody (ab179434, 1 : 3000; Abcam), IB after IP with α-FLAG (ab205606; Abcam) antibody. The total proteins were detected by α-HA (ab18181, 1 : 1000; Abcam), anti-FLAG (F-3165, 1 : 5000; Sigma) and α-MYC (ab32, 1 : 1000; Abcam) as primary antibodies. As a secondary antibody, goat anti-mouse IgG H&L (HRP) (ab205719; Abcam) was used for HA, FLAG, and MYC detection at a dilution of 1 : 5000, and goat anti-rabbit IgG H&L (HRP) (ab205718; Abcam) was used for K63 ubiquitination detection at a dilution of 1 : 5000. Protein blots were visualized as described in the previous section.

For *in vivo* ubiquitination level assays, the *ERECTApro::gERECTA-YFP er-105* and *ERECTApro::gERECTA$_{3KR}$-YFP er-105* seedlings were grown in the long-day conditions on half-strength Murashige and Skoog medium for 5 d. Total proteins were extracted from 300 mg of finely ground tissue with extraction buffer (100 mM Tris–HCl, pH 7.5, 150 mM NaCl, 1 mM EDTA, 1% Triton X-100, 1 mM PMSF, 20 μM MG132 and 1× cOmplete protease inhibitor cocktail, Sigma-Aldrich, St. Louis, MO, USA). For immunoprecipitation (IP), the total protein extracts were incubated with the GFP-Trap magnetic agarose (Cat # gtma-100; ChromoTek, Planegg-Martinsreid, Germany) at 4°C for 1 h with end-to-end rotation. After incubation, the magnetic agarose beads were separated using a magnetic rack and washed three times with washing buffer (100 mM Tris–HCl, pH 7.5, 150 mM NaCl, 1 mM EDTA, 1% Triton X-100, 1 mM PMSF, 20 μM MG132 and 1× cOmplete protease inhibitor cocktail), followed by a final wash with 50 mM Tris–HCl (pH 8.0). The amount of IP samples loaded was normalized to ensure equal GFP signal intensity, as determined by immunoblotting with anti-GFP antibody (1 : 2000, Cat # 33-2600; Invitrogen, Carlsbad, CA, USA), before ubiquitination analysis. As secondary antibody, goat anti-mouse IgG H&L (HRP) (ab205719; Abcam) was used at a dilution of 1 : 5000. Ubiquitination levels were subsequently assessed by immunoblotting with anti-Ubiquitin (linkage-specific K63) antibody (ab179434, 1 : 3000; Abcam) and anti-Ubiquitin (linkage-specific K48) antibody (ab140601, 1 : 3000; Abcam), respectively. As a secondary antibody, goat anti-rabbit IgG H&L (HRP) (ab205718; Abcam) was used at a dilution of 1 : 5000. Protein blots were visualized as described in the previous section.

Inhibitor treatment and immunoblot assays

The *ERECTApro::gERECTA-YFP er-105* and *ERECTApro::gERECTA$_{3KR}$-YFP er-105* seedlings were grown vertically at 22°C on half-strength Murashige and Skoog medium for 5 d. Thereafter, seedlings were incubated with or without endocytosis inhibitor, 50 μM Tyrphostin A23 (Tyr A23) (T7165; Sigma) for 30 min. For the vacuolar ATPase inhibitor treatment, seedlings were incubated with or without vacuolar ATPase inhibitor, 1 μM Con A (ab144227; Abcam) for 60 min. For proteasome inhibitor treatment, seedlings were incubated with or without 50 μM MG132 (M7449; Sigma) for 5 h. Total protein extracts were separated on an 8% SDS–polyacrylamide gel and detected by immunoblot analysis with anti-FLAG (F-3165, 1 : 5000; Sigma) and anti-actin (ab230169, 1 : 2000; Abcam) as primary antibodies. As a secondary antibody, goat anti-mouse IgG H&L (HRP) (ab205719; Abcam) was used at a dilution of 1 : 5000. Protein blots were visualized as described in the previous section.

Protein stability assay in protoplasts

To assess ERECTA protein stability upon ligand treatment, protoplasts cotransfected with PUB30-MYC, the wild-type ERECTA-FLAG, or the ubiquitination-mutant version ERECTA$_{3KR}$-FLAG were treated with 50 μM cycloheximide (CHX, C4859; Sigma) in the presence or absence of 5 μM mEPFL6 for 3 h. Total proteins were separated on 8% SDS–PAGE gels and transferred to the PVDF membrane (Millipore) for immunoblot analysis. ERECTA variants' protein and the input PUB30 protein were detected with α-FLAG antibody (F-3165, 1 : 5000; Sigma) and α-MYC antibody (ab32, 1 : 1000; Abcam) as primary antibodies, respectively. As a secondary antibody, goat anti-mouse IgG H&L (HRP) (ab205719; Abcam) was used at a dilution of 1 : 5000. Protein blots were visualized as described in the previous section.

RT-qPCR analysis

Tissues for qPCR analysis were harvested at 4 d old for established lines. RNA extraction, cDNA synthesis, and RT-qPCR were performed as described previously (Pillitteri *et al.*, 2011). Transcript levels were normalized against the housekeeping gene *ACTIN* (*ACT2*). For primer DNA sequences used for RT-qPCR analysis, see Table S2.

Phylogenetic analysis

The full-length amino-acid sequences of the AtERECTA, AtERL1, AtERL2 as well as ERECTA orthologs across land plants were retrieved as reported previously (Chen *et al.*, 2023), and they were subjected to alignment using ClustalW. See Data availability statement for all accession numbers. The generated alignment file was examined for a gap-sequence, then visualized using Jalview (http://www.jalview.org/), with amino-acid residues color coded according to the ClustalX colors scheme.

Results

Ubiquitination-deficient ERECTA overly inhibits stomatal development

The loss-of-function *erecta* mutant exhibits an increased number of small stomatal lineage cells (Shpak *et al.*, 2005; Lee *et al.*, 2012). By contrast, the *pub30pub31* double mutant overly reduces stomatal development (Chen *et al.*, 2023). We hypothesized that the expression of ubiquitination-deficient ERECTA in the *erecta* null mutant (*er-105*) background leads to over-inhibition of stomatal development. A previous large-scale profiling of the Arabidopsis membrane-protein ubiquitome has identified a single lysine residue (K668) within the ERECTA

© 2026 The Author(s).
New Phytologist © 2026 New Phytologist Foundation.

kinase domain as a ubiquitination site (Grubb *et al.*, 2021). With this in mind, we generated an epitope-tagged version of ERECTA in which K668 was substituted with arginine via site-directed mutagenesis ($ERECTA_{K668R}$) and conducted a functional complementation assay (Fig. 1). However, *ERECTApro::ERECTA$_{K668R}$-FLAG* failed to confer the over-complementation phenotype, indicating that there are other functionally relevant ubiquitination sites in ERECTA (Fig. 1a,b).

To explore potential ubiquitination sites within the juxtamembrane region of ERECTA, we performed sequence alignment among ERECTA family members, including Arabidopsis ERL1 and ERL2, and selected ERECTA orthologs across the land plant lineages. The known ERECTA ubiquitination, K668, is conserved throughout the ERECTA family members examined (Fig. 2a). Likewise, we found that K625 is deeply conserved from moss, liverwort, to monocot and dicot ERECTA orthologs as well as Arabidopsis ERL1/2 (Fig. 2a). The K617 residue is highly conserved among the ERECTA orthologs while not conserved in Arabidopsis ERLs (Fig. 2a).

We subsequently mutated each site in combination with the previously reported site (K668) to generate higher-order ERECTA variants ($ERECTA_{K617RK668R}$ or $ERECTA_{K625RK668R}$, hereby $ERECTA_{2KR617}$ and $ERECTA_{2KR625}$). Both *ERECTApro::ERECTA$_{2KR617}$-FLAG* and *ERECTApro::ERECTA$_{2KR625}$-FLAG* produced a reduced number of stomata and meristemoid compared to the control *ERECTApro:: ERECTA-FLAG* lines, suggesting that these two residues are additional ubiquitination sites in ERECTA (Figs 1b, 2c). To assess the protein stability of these ubiquitination mutant variants, we examined the abundance of ERECTA variants in the presence of the proteasome inhibitor MG132 (see the Materials and Methods section). Before treatment, the $ERECTA_{2KR617}$ and $ERECTA_{2KR625}$

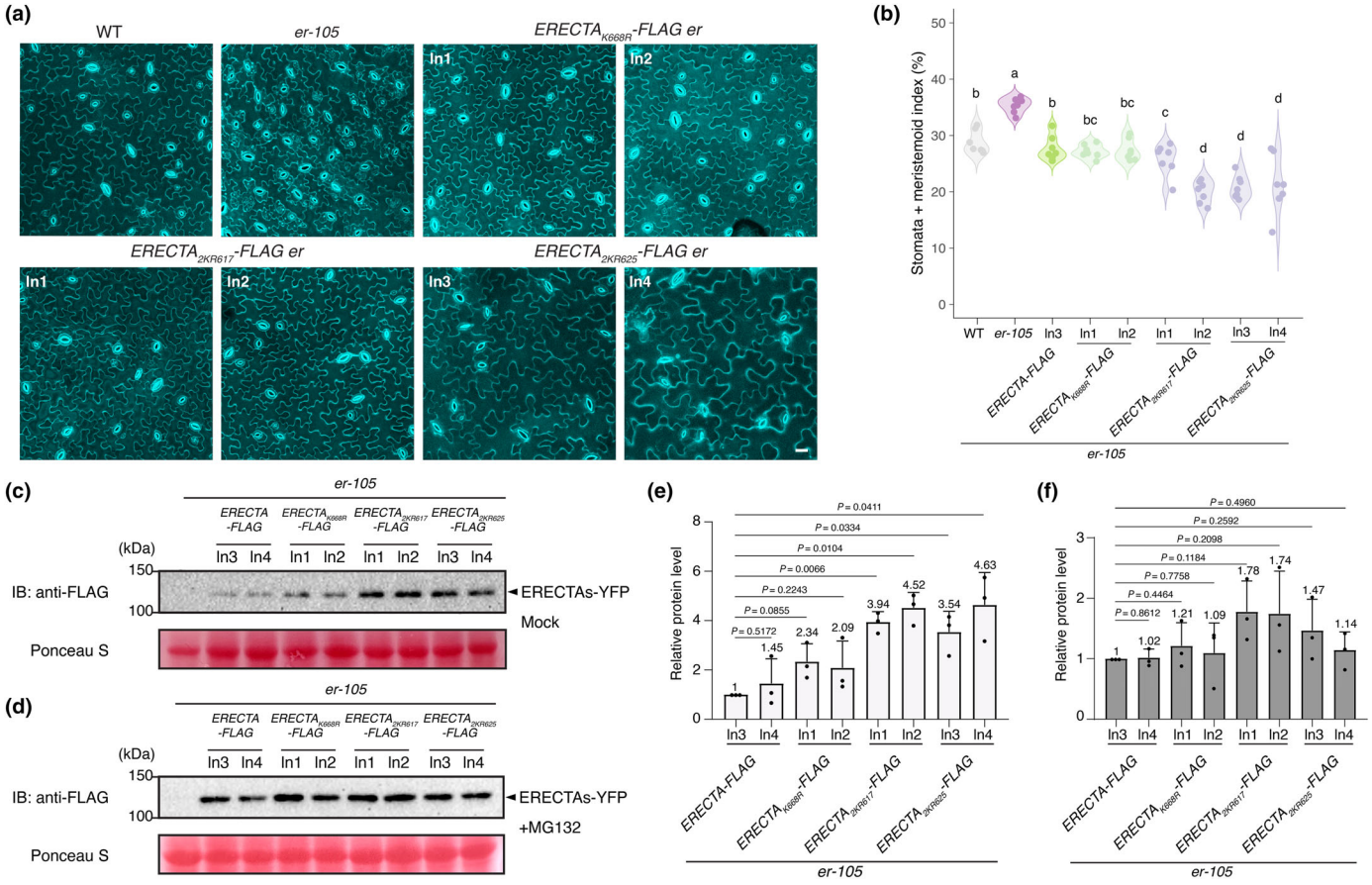
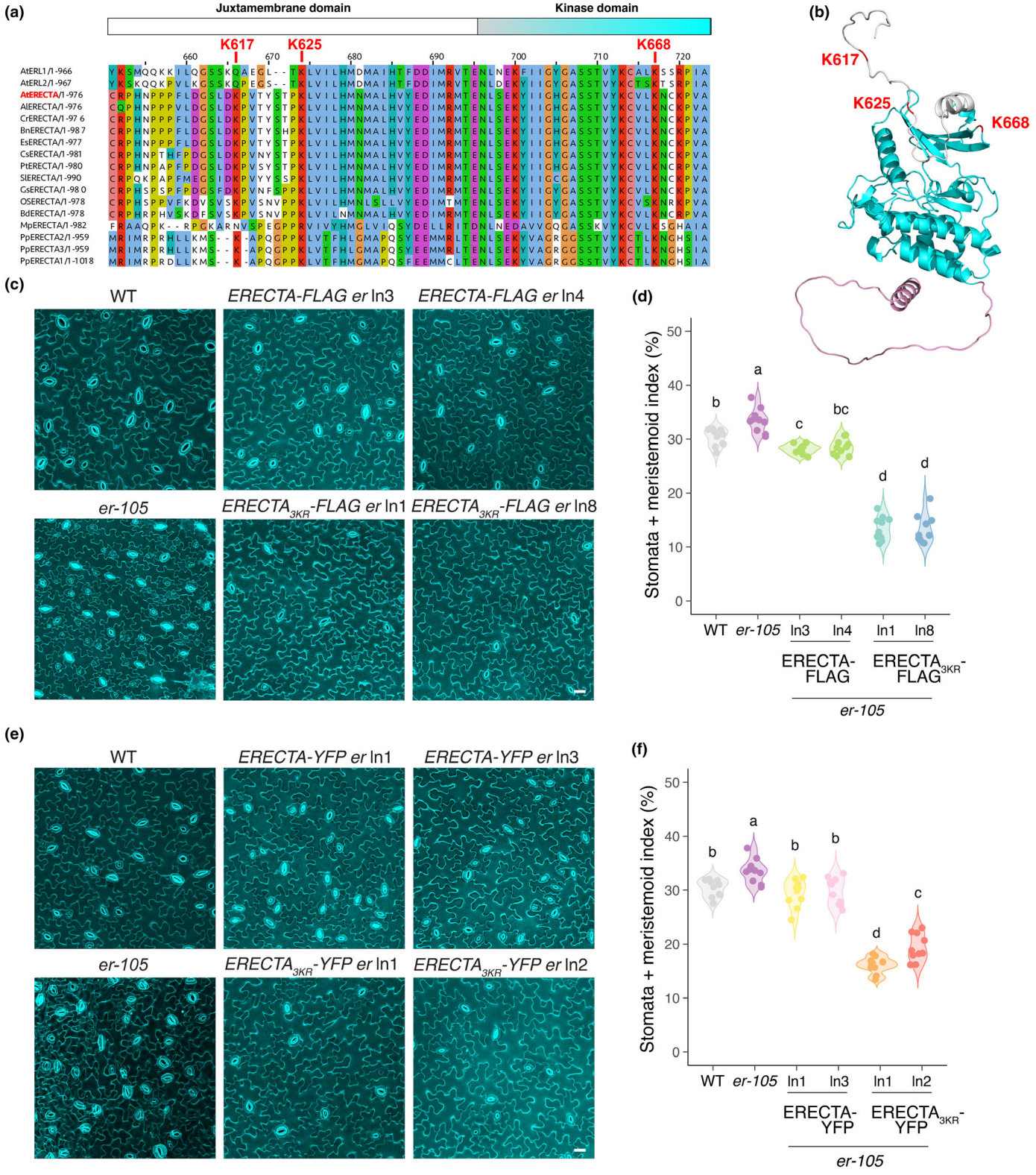


Fig. 1 Mutations of predicted lysine residues in ERECTA show redundancy in inhibiting stomatal development in *Arabidopsis thaliana*. (a) Representative confocal microscopy of cotyledon abaxial epidermal from 7-d-old wild-type (WT), *er-105* (*er*), *ERECTA$_{K668R}$-FLAG er*, *ERECTA$_{2KRK617}$-FLAG er*, and *ERECTA$_{2KRK625}$-FLAG er*. The same representative transgenic lines were observed. Images were taken under the same magnification. Bar, 25 μm. (b) Quantitative analysis. Stomata + meristemoid index (number of stomata and meristemoid per 100 epidermal cells) of the cotyledon abaxial epidermis from 7-d-old seedlings of respective genotypes ($n = 7$). Data are presented as violin plots where the width represents data density and all individual data points are displayed to show the full distribution. One-way ANOVA followed by Tukey's HSD test was performed, and statistically different groups are labeled with distinct letters (e.g. a, b, c, d), while groups labeled with the same letter are not statistically different from each other ($P < 0.05$). (c, d) Protein accumulation of ERECTA variants described in (a), treated with (+MG132) and without (−MG132) proteasome inhibitor MG132. Total proteins were isolated from 5-d-old seedlings and probed by an α-FLAG antibody. (e, f) Quantification of protein abundance (ERECTAs/Rubisco) ($n = 3$ biological replicates) in the absence and presence of MG132. Welch's unpaired *t*-tests were performed, and the corresponding *P*-values were labeled on the plots. Bars represent mean ± SD.

© 2026 The Author(s).
New Phytologist © 2026 New Phytologist Foundation.

variants exhibited significantly higher protein levels compared to the wild-type version, whereas the ERECTA$_{K668R}$ variant remained comparable to the control (Fig. 1c,e). MG132 treatment stabilized all ERECTA variants to similar levels (Fig. 1d,f), suggesting that the observed phenotypes may result from impaired ubiquitin-mediated degradation of these specific mutants. We therefore substituted all three lysine residues with arginine residues (ERECTA$_{K617RK625RK668R}$, hereafter



© 2026 The Author(s).
New Phytologist © 2026 New Phytologist Foundation.

Fig. 2 Ubiquitination-deficient ERECTA overly inhibits stomatal development in *Arabidopsis thaliana*. (a) Sequence alignment of the cytoplasmic domain of ERECTA (ERECTA_CD) across the ERECTA orthologs and Arabidopsis paralogs: AtERL1 (AT5G62230.1), AtERL2 (AT5G07180.1), AtERECTA (AT2G26330.1), *Arabidopsis lyrata* AlERECTA (XP_020884443.1), *Capsella rubella* CrERECTA (XP_006296065.1), *Brassica napus* BnERECTA (AGL91677.1), *Eutrema salsugineum* EsERECTA (XP_006408746.1), *Glycine soja* GsERECTA (KHN37058.1), *Solanum lycospersicum* SlERECTA (XP_004245043.1), *Poplus trichocarpa* PtERECTA (XP_024458576.1), *Oryza sativa cv japonica* OsERECTA (XP_015642019.1), *Brachypodium distachyon* BdERECTA (KQK19116.1), Marchantia polymorpha MpERECTA (Mapoly0070s0019.1), and *Physcomitrella patens* PpERECTA1 (Pp3c2_22410V3.1), PpERECTA2 (Pp3c1_17360V3.1), and PpERECTA3 (Pp3c21_9500V3.1). Juxtamembrane domains are highlighted in white, and the Kinase domains are in cyan. Each residue in the alignment is color coded according to the ClustalX color scheme in Jalview based on properties and conservation (see the Materials and Methods section). The selected lysine residues are labeled. (b) Structural modeling of the cytoplasmic domain of ERECTA, with the Juxtamembrane domain in light gray and the Kinase domain in cyan. (c) Representative confocal microscopy of cotyledon abaxial epidermis from 7-d-old wild-type (WT), *er-105* (*er*), *ERECTA-FLAG er*, and *ERECTA$_{3KR}$-FLAG er*. The same representative transgenic lines were observed. Images were taken under the same magnification. Bar, 25 μm. (d) Quantitative analysis. Stomata + meristemoid index (number of stomata and meristemoids per 100 epidermal cells) of the cotyledon abaxial epidermis from 7-d-old seedlings of respective genotypes (n = 10). Data are presented as violin plots where the width represents data density and all individual data points are displayed to show the full distribution. One-way ANOVA followed by Tukey's HSD test was performed, and statistically different groups are labeled with distinct letters (e.g. a, b, c, d), while groups labeled with the same letter are not statistically different from each other ($P < 0.05$). (e) Representative confocal microscopy of cotyledon abaxial epidermal from 7-d-old wild-type (WT), *er-105* (*er*), *ERECTA-YFP er*, and *ERECTA$_{3KR}$-YFP er*. The same representative transgenic lines were observed. Images were taken under the same magnification. Bar, 25 μm. (f) Quantitative analysis. Stomata + meristemoid index of the cotyledon abaxial epidermis from 7-d-old seedlings of respective genotypes (n = 10). Data are presented as violin plots where the width represents data density, and all individual data points are displayed to show the full distribution. One-way ANOVA followed by Tukey's HSD test was performed, and statistically different groups are labeled with distinct letters (e.g. a, b, c, d), while groups labeled with the same letter are not statistically different from each other ($P < 0.05$).

ERECTA$_{3KR}$). As expected, the expression of *ERECTApro::ERECTA$_{3KR}$-FLAG* led to over-rescue phenotypes in stomatal development and pedicel elongation, with significantly reduced SMI (stomatal + meristemoid index = (number of stomata + meristemoid)/total number of epidermal cells × 100) and vastly increased pedicel length (Figs 2c,d, S1). Consistently, the expression of *ERECTApro::ERECTA$_{3KR}$-YFP* also led to repressed stomatal development and enhanced pedicel growth (Figs 2e,f, S1). Transcript levels of the transgenes are comparable among the transgenic lines, either expressing *ERECTA-FLAG* and *ERECTA$_{3KR}$-FLAG* (Fig. S2A) or *ERECTA-YFP* and *ERECTA$_{3KR}$-YFP* (Fig. S2B), indicating that the observed excessive phenotypic rescues are not attributable to the transgene overexpression. Combined, the data suggest that multiple lysine residues cooperatively regulate ERECTA activity via ubiquitination and that ubiquitination on ERECTA plays a positive role in stomatal development.

K63-linked polyubiquitination of ERECTA by PUB30 and PUB31 is reduced in the predicted ubiquitination site mutant versions

To confirm that these lysine residues are the major ubiquitination sites, we first performed *in vitro* ubiquitination assays with recombinant ERECTA cytoplasmic domain fused with maltose binding protein (MBP-ERECTA_CD) as well as its triple lysine-to-arginine substitution version (MBP-ERECTA_CD$_{3KR}$) as substrates. The ubiquitination of MBP-ERECTA_CD$_{2KR617}$, MBP-ERECTA_CD$_{2KR625}$, and MBP-ERECTA_CD$_{3KR}$ by PUB30/PUB31 was much weaker than that of MBP-ER_CD (Figs 3a, S3A,B), suggesting that PUB30/PUB31 ubiquitinates ERECTA at the K617, K625, and K668 residues. E2 ubiquitin–conjugating enzymes (UBCs) act as key mediators of ubiquitin chain assembly, and E3 ligases show pairing specificity with different E2s (Kraft *et al.*, 2005; Turek *et al.*, 2018; Trujillo, 2021). We then tested the auto-ubiquitination of PUB30 by UBC35, a major E2 for K63-linked polyubiquitination of plant membrane proteins (Turek *et al.*, 2018; Saeed *et al.*, 2023), and UBC8, which has been routinely utilized to activate PUB12/13 for ubiquitination assays of FLS2 and BRI1 (Lu *et al.*, 2011; Zhou *et al.*, 2018). Both UBC35 and UBC8 exhibited comparable activity for auto-ubiquitination of PUB30 (Fig. S3C), suggesting that E2 enzyme specificity may be more restricted under *in vivo* conditions.

To address the *in vivo* role of these lysine residues in regulating ERECTA, we next compared the *in vivo* ubiquitination status of ERECTA and ERECTA$_{3KR}$ in *er-105*, complemented with *ERECTApro::ERECTA-YFP* and *ERECTApro::ERECTA$_{3KR}$-YFP* seedlings, respectively (Fig. 3b). Total proteins were extracted and subjected to anti-GFP immunoprecipitation, followed by immunoblotting with K48- and K63-linkage specific polyubiquitin antibodies, respectively. Neither wild-type ERECTA-YFP nor ERECTA$_{3KR}$-YFP immunoprecipitates showed discernible signal, suggesting that ERECTA is not tagged by K48-linked poly-ubiquitination (Fig. 3b). By contrast, immunoprecipitated wild-type ERECTA-YFP showed K63-linked poly-ubiquitination signals, a well-established signal for the internalization of membrane proteins in plants (Saeed *et al.*, 2023). The K63 poly-ubiquitination signal was markedly reduced in ERECTA$_{3KR}$-YFP (Figs 3b, S3D). The immunoprecipitated, lower-molecular-weight bands detected by the K63-linked poly-ubiquitin antibody likely represent cleaved ERECTA fragments retaining the K63-ubiquitin chains (Fig. 3b, asterisks). Again, such bands are not detected in ERECTA$_{3KR}$-YFP, indicating that these three lysine residues are subjected to the K63 poly-ubiquitination.

Next, we sought to investigate whether this K63-ubiquitination of ERECTA is triggered by ligand perception. For this purpose, we utilized recombinant, mature EPFL6 peptide, mEPFL6. Among the EPF/EPFL peptide family, EPFL6 is known to regulate ERECTA functions in internal tissues (e.g.

© 2026 The Author(s).
New Phytologist © 2026 New Phytologist Foundation.

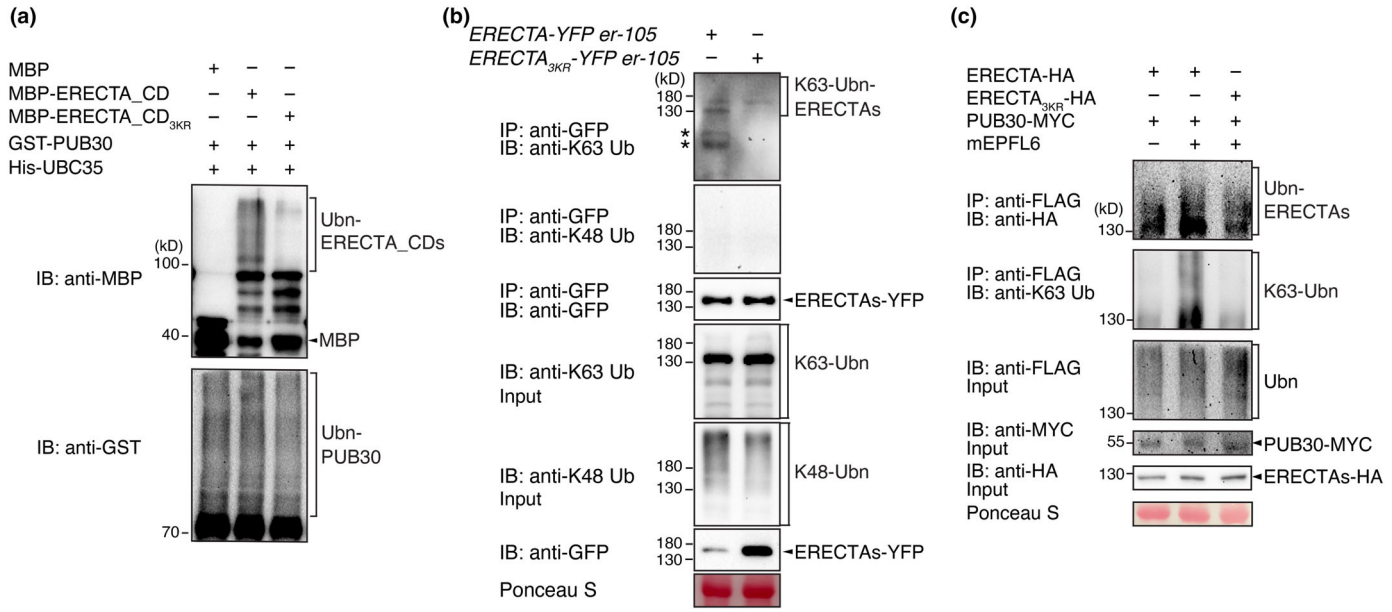


Fig. 3 The predicted ubiquitination sites are required for the K63-linked polyubiquitination of ERECTA. (a) Lysines K617, K625, and K668 are required for the ubiquitination of ERECTA by PUB30 *in vitro*. The ubiquitination of MBP-ERECTA_CD or MBP-ERECTA_CD$_{3KR}$ was carried out by using GST-fused PUB30 as the E3 ligase, His-fused AtUBA1 as the E1 activating enzyme, and His-fused UBC35 as the E2 conjugating enzyme. (b) Reduced K63-linked polyubiquitination in Arabidopsis ERECTA$_{3KR}$ variant. IP was performed using α-GFP antibodies on total protein extracts from homozygous plants expressing ERECTA-YFP or ERECTA$_{3KR}$-YFP and the immunoblots (IB) were probed with anti-K63-linked ubiquitin and anti-GFP antibodies, respectively. (c) Lysines K617, K625, and K668 are required for the ubiquitination of ERECTA by PUB30 *in vivo*. Arabidopsis protoplasts were cotransfected with HA-tagged ERECTAs (ERECTA-HA or ERECTA$_{3KR}$-HA), FLAG-tagged ubiquitin (FLAG-UBQ), and together with MYC-tagged PUB30 and incubated for 10 h followed by treatment with 5 μM mEPFL6 for 1 h in the presence of 5 μM MG132. After immunoprecipitation using anti-FLAG beads, the ubiquitinated ERECTA or ERECTA$_{3KR}$ was probed with α-HA antibody. The total ubiquitinated proteins were probed by an α-FLAG antibody and PUB30 protein was probed by an α-MYC antibody. The input levels of ERECTA or ERECTA$_{3KR}$ were probed with α-HA antibody.

endodermis and vasculature) as well as in the epidermis (Abrash & Bergmann, 2010; Uchida *et al.*, 2012). Thus, we presumed that mEPFL6 could trigger more robust ubiquitination signals on ERECTA protein pools during whole seedling protein extraction. *In vivo* ubiquitination assay was carried out in *Arabidopsis* protoplasts upon bioactive mature EPFL6 (mEPFL6) peptide treatment. Laddering bands with high-molecular-mass proteins were observed following immunoprecipitation (Fig. 3c), indicating that ERECTA undergoes K63 polyubiquitination *in vivo*. Strikingly, the ubiquitination of ERECTA$_{3KR}$-HA by PUB30 was reduced compared with wild-type ERECTA-HA (Fig. 3c). Notably, the K63 linkage-specific ubiquitination of ERECTA$_{3KR}$-HA by PUB30 was impaired (Fig. 3c). Based on these results, we conclude that the three lysine residues within the cytoplasmic domain of ERECTA, K617, K625, and K668, are the major K63-linked ubiquitination sites of ERECTA by its E3-ligase PUB30/PUB31 and are responsible for its eventual degradation.

Ubiquitination-deficient ERECTA displays reduced ligand-induced endocytosis

Modification of plasma membrane proteins with K63-ubiquitin chains impacts their endocytosis (Foot *et al.*, 2017; Aniento *et al.*, 2021; Saeed *et al.*, 2023). Based on our results, we hypothesized that the K63-ubiquitination sites of ERECTA regulate its endocytosis. We therefore examined the subcellular behaviors of ERECTA-YFP as well as its ubiquitination-deficient version ERECTA$_{3KR}$-YFP. As shown in Fig. 4(a,c), we detected ERECTA-YFP-labeled punctae that co-localized with FM4-64, a styryl dye for tracing endocytic pathways in plants (Meckel *et al.*, 2004), suggesting that ERECTA is actively undergoing endocytosis. Compared to the wild-type ERECTA-YFP, ERECTA$_{3KR}$-YFP exhibits strong, brighter YFP fluorescence signals at the plasma membrane owing to its increased stability (Fig. 4a,b). Nevertheless, the number of ERECTA$_{3KR}$-YFP endosomes is significantly reduced (Fig. 4b,c).

To delineate which specific subcellular route is impacted by the loss of proper K63-ubiquitination of ERECTA, we next performed a pharmacological approach using Wortmannin (Wm), an inhibitor of phosphatidylinositol-3 (PI3) and phosphatidylinositol-4 (PI4) kinases (Foissner *et al.*, 2016). Wm treatment causes a fusion of provacuolar compartments to form multivesicular bodies (MVB), also known as Wm bodies (Wang *et al.*, 2009). The Wm application resulted in the formation of typical ring-like Wm bodies marked by both ERECTA-YFP and FM4-64 (Fig. 4a,d). Notably, many fewer Wm bodies were observed in ERECTA$_{3KR}$-YFP seedlings than in the WT ERECTA-YFP background (Fig. 4b,d).

To define the subcellular localization of endocytosed ERECTA-YFP and the specific location impacted by the lack of K63-ubiquitination, we next examined the co-localization of

© 2026 The Author(s).
New Phytologist © 2026 New Phytologist Foundation.

ERECTA with intracellular trafficking marker proteins. Specifically, we observed co-localization of wild-type and K63-ubiquitination-deficient ERECTA-YFP fusions with RFP-ARA6 for MVB/LE (late endosomes) and plasma membrane and SYP43-RFP for *trans*-Golgi network/early endosomes (TGN/EEs) (Ebine *et al.*, 2011; Postma *et al.*, 2016). ERECTA-YFP extensively co-localizes and moves together with RFP-ARA6 (Fig. 4g). Similarly, ERECTA-YFP-labeled punctae are also labeled by SYP43-RFP (Fig. 4h). Notably, much reduced co-localization signals were observed in $ERECTA_{3KR}$-YFP seedlings (Fig. 4g–i), further confirming that endocytosed ERECTA-YFP predominantly resides on the TGN/EEs and MVB/LE and that K63-linked ubiquitination of ERECTA is essential for its endocytosis.

It has been reported that EPF1 and EPFL6, ligands of ERECTA-family receptors, trigger the internalization of ERL1 and that EPF2/EPFL6 application triggers the ubiquitination of ERECTA by PUB30/31 (Qi *et al.*, 2020; Chen *et al.*, 2023). Because EPF2 is the natural ligand of ERECTA for epidermal stomatal patterning (Lee *et al.*, 2012), we employed EPF2 for internalization assays to specifically monitor ERECTA endocytosis during stomatal development. We therefore asked whether the ligand-induced endocytosis of ERECTA depends on its ubiquitination. For this purpose, we took advantage of the biologically active mature EPF2 (mEPF2) peptides (Fig. 4a,b; Lee *et al.*, 2012; Qi *et al.*, 2017, 2020; Chen *et al.*, 2023). The application of mEPF2 intensified the number of ERECTA-YFP-labeled endosomes per area, especially more evident when the ligand was applied together with Wm (Fig. 4a,c,d). By contrast, the ligand application failed to induce $ERECTA_{3KR}$-YFP-labeled endosomes (Fig. 4b–d), further suggesting that ubiquitination of ERECTA is a prerequisite for its ligand-induced endocytosis.

K63-linked ubiquitination is required for eventual vacuolar degradation of ERECTA

Receptors that are internalized through MVB/LE pathways are eventually targeted for degradation in the lytic vacuole (Reyes *et al.*, 2011). We examined whether the ubiquitination-induced endocytosis of ERECTA is the major path for ERECTA protein degradation *in vivo*. Consistent with previous results (Fig. 4), higher accumulation of $ERECTA_{3KR}$ ($ERECTA_{3KR}$-YFP) was detected compared with the wild-type ERECTA (ERECTA-YFP) (Fig. 5a,b). By contrast, the transcriptional levels were not significantly different between wild-type ERECTA and $ERECTA_{3KR}$ seedlings (Fig. S2B), suggesting that the effects of $ERECTA_{3KR}$ accumulation are indeed posttranslational.

To further assess whether endocytic/vacuolar degradation pathways are responsible for the enhanced protein abundance of $ERECTA_{3KR}$-YFP, we subsequently treated the seedlings with Tyrphostin A23 (Tyr A23) and Concanamycin A (Con A). Tyr A23 is an inhibitor of clathrin-mediated endocytosis owing to its activity as a membrane uncoupler that triggers cytoplasmic acidification (Santuari *et al.*, 2011; Dejonghe *et al.*, 2016) and Concanamycin A (Con A) is a vacuolar ATPase inhibitor that is known to diminish protein degradation in the lytic vacuole (Kleine-Vehn *et al.*, 2008). As shown in Figs 5(a,b) and S4, treatments of both Tyr A23 and Con A resulted in a significant increase in ERECTA protein accumulation, but not in that of the K63-ubiquitination deficient $ERECTA_{3KR}$. We furthermore observed that ERECTA-YFP accumulates within the tonoplast, as confirmed by FM4-64 staining following Concanamycin A treatment (Fig. 4e). By contrast, $ERECTA_{3KR}$-YFP was strongly retained at the PM and failed to undergo vacuolar deposition (Fig. 4f). These observations further highlight the direct role of ERECTA ubiquitination in its internalization from the PM to the eventual vacuolar destination.

Finally, we tested the function of K63-ubiquitination on the ligand-induced degradation of ERECTA protein. For this purpose, we co-expressed ERECTA or $ERECTA_{3KR}$, and PUB30 in Arabidopsis protoplast and performed co-treatment with mEPFL6 and cycloheximide (CHX, *de novo* protein synthesis inhibitor). Upon mEPFL6 treatment, ERECTA-FLAG showed a significant decrease in protein level (Fig. 5c,d). By contrast, PUB30-MYC conferred a smaller reduction of $ERECTA_{3KR}$-FLAG protein level (Fig. 5c,d). Taken together, our results thus demonstrate that ubiquitination-induced endocytosis of ERECTA triggers its vacuolar degradation.

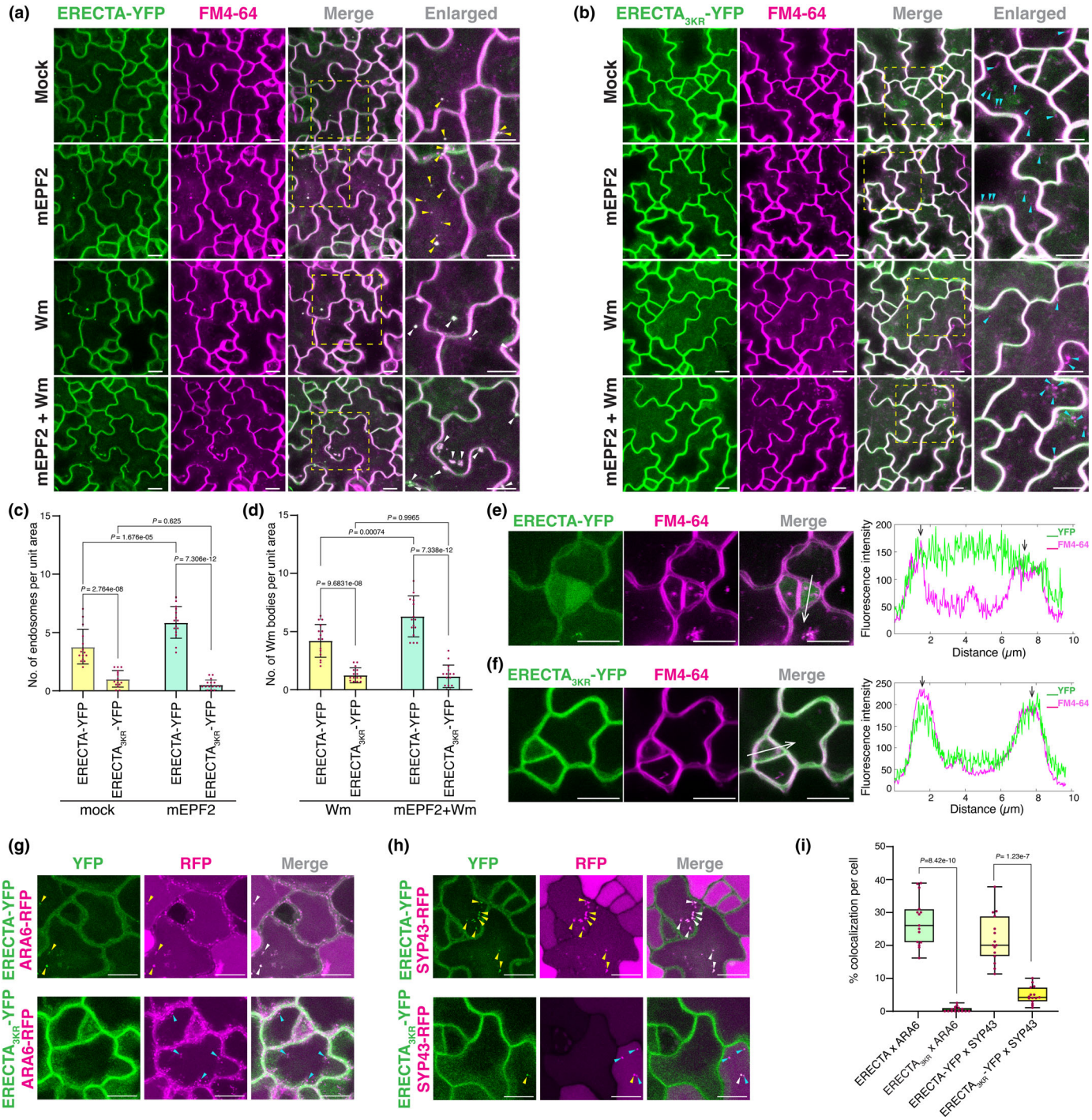
Discussion

Our previous study identified two PUB-type E3 ligases, PUB30 and PUB31, as key attenuators of the ERECTA regulatory circuit, which ensure optimal signal outputs. Recently, K63-ubiquitin chains have been reported to serve as a general signal for early endocytosis of integral plasma membrane proteins, including FLS2, BRI1, and PIN1 (Saeed *et al.*, 2023). However, the type of ubiquitin linkage on ERECTA and its connection to receptor turnover has remained unclear. In this study, we identify K63-linked ubiquitination of ERECTA as a key regulatory mechanism that controls its internalization and vacuolar degradation during stomatal development, as well as during inflorescence and pedicel elongation. Perception of EPF/EPFL peptides initiates a defined signaling cascade through heterodimerization with BAK1/SERKs, leading to suppression of a transcription factor that drives stomatal lineage initiation (Lampard *et al.*, 2008; Horst *et al.*, 2015; Meng *et al.*, 2015). To preserve signal fidelity and spatial restriction, receptor activity must be tightly regulated. Our data show that PUB30/PUB31-mediated K63-linked ubiquitination promotes the internalization and degradation of ERECTA upon ligand activation (Fig. 6). By mapping and validating three lysine residues essential for this modification, we show that K63-linked ubiquitination is required for ligand-induced endocytosis and subsequent protein degradation of ERECTA, thereby preventing excessive or prolonged receptor activity. These findings provide mechanistic insight into how post-translational control of plasma membrane-localized RLKs contributes to precise signaling during plant development.

Our sequence alignment revealed that the location of two lysine residues (K617 and K625) within its juxtamembrane domain is conserved in ERECTA orthologs and paralogs, in addition to the previously known ubiquitination site within the kinase domain, K668 (Fig. 2a). Correspondingly, our site-

© 2026 The Author(s).
New Phytologist © 2026 New Phytologist Foundation.

directed mutagenesis of the lysine residues K617R and K625R within the juxtamembrane of ERECTA together with the known ubiquitination site conferred stable protein accumulation and hyperactivity of ERECTA signaling. These results support a role for the juxtamembrane domain of ERECTA as a ubiquitination-targeted domain in controlling receptor stability. Consistently, we previously observed that the truncated ERECTA protein lacking the entire cytoplasmic domain, including the juxtamembrane domain, stably accumulates at the plasma membrane and confers strong dominant-negative effects (Shpak *et al.*, 2003). Likewise, the dominant-negative ERL1, which also lacks the entire cytoplasmic domain, triggers stable accumulation at the plasma membrane (Qi *et al.*, 2020), suggesting that the ubiquitination-dependent regulation occurs in other ERECTA-



© 2026 The Author(s).
New Phytologist © 2026 New Phytologist Foundation.

Fig. 4 The ubiquitination of Arabidopsis ERECTA is required for ligand-induced endocytic trafficking. (a, b) Representative confocal images of ERECTA-YFP (a) and ERECTA$_{3KR}$-YFP (b) in the epidermis of 4-d-old seedlings co-stained with 8 μM FM4-64 (magenta), following 5 μM mEPF2 peptide and 30 μM Wm treatment for 90 min. Arrowheads in yellow indicate ERECTA-YFP endosomes co-localizing with FM4-64 stains. Arrowheads in white indicate Wm bodies of FM4-64 co-localizing with ERECTA-YFP. Arrowheads in cyan indicate the FM4-64 endosomes that do not co-localize with ERECTA$_{3KR}$-YFP signals. The enlarged views are shown in the yellow dashed boxes. The images were collected as Z-stacks. Bars, 10 μm. (c) Quantification of endosome number per unit area (82 μm × 82 μm) in ERECTA-YFP and ERECTA$_{3KR}$-YFP with or without 5 μM mEPF2 treatment. Each dot represents the average number of endosomes per image (three images per seedling, n = 15 seedlings). Welch's unpaired t-tests were performed, and the corresponding P-values were labeled on the plots. Bars represent mean ± SD. (d) Quantification of Wm bodies number per unit area in ERECTA-YFP and ERECTA$_{3KR}$-YFP seedlings treated with 30 μM Wm, along with or without 5 μM mEPF2 treatment. Each dot represents the number of Wm bodies per image. Each dot represents the average number of endosomes per image (three images per seedling, n = 15 seedlings). Welch's unpaired t-tests were performed, and the corresponding P-values were labeled on the plots. (e, f) Representative confocal images showing ERECTA-YFP, ERECTA$_{3KR}$-YFP (green) and FM4-64 (tonoplast, magenta) in the epidermis of 4-d-old seedlings after 6 h of 1 μM Concanamycin A treatment. Tonoplast is stained by FM4-64. The white arrow indicates the line plots of YFP and RFP fluorescence on 10-pixel thickness in the right panels. The black arrow in the right panel indicates FM4-64 fluorescent highlighting the tonoplast. The images were collected as Z-stacks. Bars, 10 μm. (g, h) Representative confocal images showing co-localization of ERECTA-YFP (e) and ERECTA$_{3KR}$-YFP (f) analysis with MVB/LE marker ARA6 (g) and TGN/EEs marker SYP43 (h) in the epidermis of 4-d-old seedlings. Merged images are shown in the right panel. Yellow arrows indicate the endosomes bearing ERECTA-YFP, ERECTA$_{3KR}$-YFP, ARA6-RFP and SYP43-RFP. White arrows point to the co-localization between ERECTA-YFP, ERECTA$_{3KR}$-YFP and the markers. Cyan arrows indicate the endosomes labeled only with the markers, without ERECTA$_{3KR}$-YFP. The images were collected as Z-stacks. Bars, 10 μm. (i) Quantification of endosome numbers in ERECTA-YFP and ERECTA$_{3KR}$-YFP co-localizing with ARA6-RFP and SYP43-RFP markers. Percentage of the co-localized endosomes between ERECTA-YFP and ERECTA$_{3KR}$-YFP and endosome markers in each image is shown as dots (10 cells per image, n = 15 images). Welch's unpaired t-tests were performed, and the corresponding P-values were labeled on the plots. Boxplots show median values (center bar), first and third quartile (box), and 1.5 times the interquartile range (whiskers).

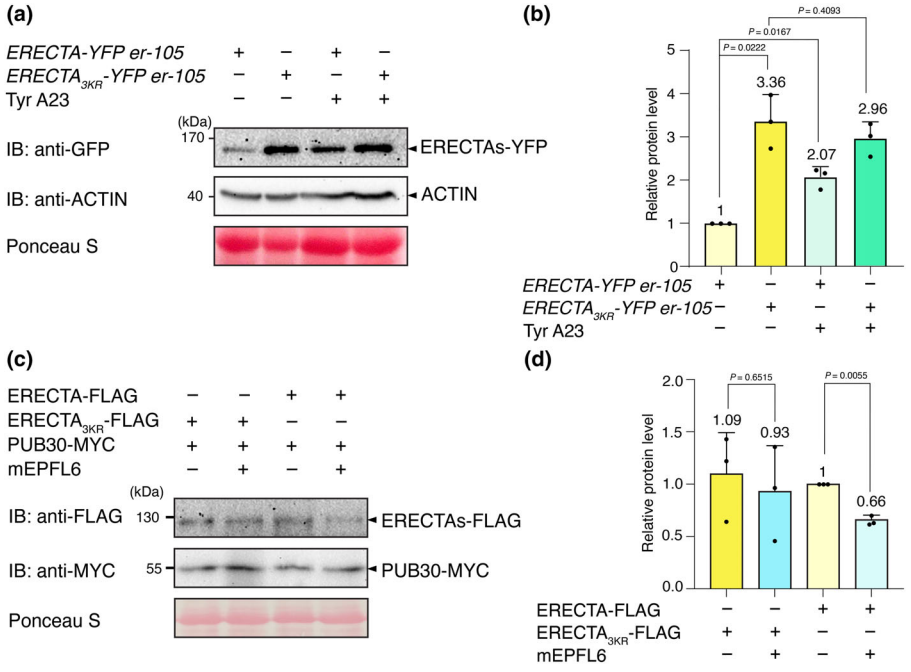


Fig. 5 K63-linked ubiquitination is required for eventual vacuolar degradation of Arabidopsis ERECTA. (a) Protein accumulation in *ERECTA-YFP er-105 (er)* and *ERECTA$_{3KR}$-YFP er*, in the absence and presence of the endocytosis inhibitor Tyrphostin A23 (Tyr A23). Total proteins were isolated from 5-d-old seedlings and probed by an α-GFP antibody. The protein inputs were equilibrated using α-Actin antibodies. (b) Quantification of protein abundance (ERECTA/Actin and *ERECTA$_{3KR}$*/Actin) (n = 3 biological replicates) in the absence and presence of Tyr A23. Welch's unpaired t-tests were performed, and the corresponding P-values were labeled on the plots. Bars represent mean ± SD. (c) Lysines K617, K625, and K668 are required for the destabilization of ERECTA-FLAG after mEPFL6 application in Arabidopsis protoplasts co-expressing FLAG-tagged ERECTAs (ERECTA-FLAG or ERECTA$_{3KR}$-FLAG) together with MYC-tagged PUB30. Protoplasts expressing the indicated proteins were treated with 50 μM CHX and 5 μM mEPFL6 for 3 h before total protein was examined with an immunoblot. (d) Quantification of protein abundance (ERECTA/Rubisco and *ERECTA$_{3KR}$*/Rubisco) (n = 3 biological replicates) in the absence and presence of mEPFL6. Welch's unpaired t-tests were performed, and the corresponding P-values were labeled on the plots. Bars represent mean ± SD.

family RKs. Further structural analyses may elucidate the modular functions of ERECTA cytoplasmic domains (Fig. 2b). The finding that ERECTA$_{3KR}$ (K617R, K625R, and K668R) exhibits the strongest phenotypes, both in stomatal development and pedicel elongation, suggests that ubiquitination outside of the juxtamembrane domain can further contribute to receptor

© 2026 The Author(s).
New Phytologist © 2026 New Phytologist Foundation.

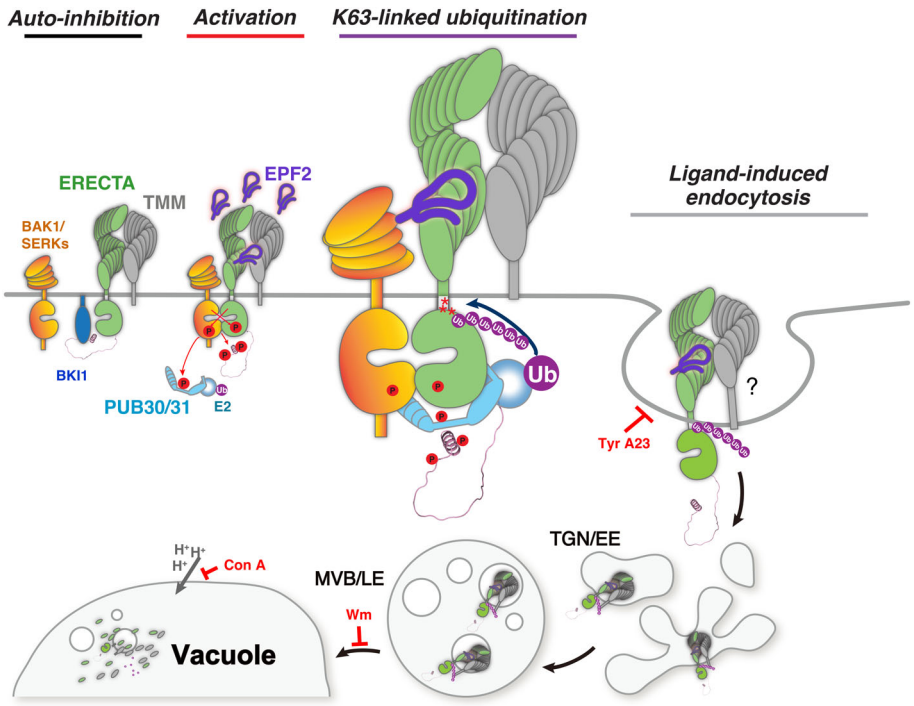


Fig. 6 Schematic model of ERECTA endocytosis and homeostasis regulated by ligand-induced ubiquitination during stomatal development. Initially, BKI1 (blue) associates with ERECTA (green) in the absence of ligand, and ERECTA is in the basal state (*Auto-inhibition*). Upon perception of the ligand EPF2 (violet), ERECTA signaling becomes activated (red arrows). The formation of the receptor complex, ERECTA and its co-receptors TMM (gray) and BAK1/SERKs (orange), initiates signal transduction that ultimately restricts stomatal development (*Activation*). Following activation, ERECTA is ubiquitinated at lysine residues K617, K625, and K668 via PUB30/31 (cyan) (*K63-linked polyubiquitination*). Thereafter, the ubiquitinated ERECTA undergoes endocytosis and vacuolar/lysosomal degradation (black arrows), which maintains appropriate receptor homeostasis to ensure proper stomatal development (*Ligand-induced endocytosis*). Whether TMM (gray) co-internalizes with ERECTA upon ligand perception remains to be investigated. Red T-bars indicate the site of action of each pharmacological inhibitor used in this study.

internalization. Our phylogenetic sequence analysis revealed a deep conservation of these lysine sites among the ERECTA orthologs across the land plant lineages. Thus, the regulation of ERECTA functions and dynamics by ubiquitination may be conserved beyond Arabidopsis.

In plants, the endosomal sorting complex required for transport (ESCRT) component, such as VPS23A, is tagged by K48-linked polyubiquitin, targeting them for proteasomal degradation (Hasegawa *et al.*, 2024). By contrast, BRI1 is modified by K63-linked, not K48-linked, ubiquitins *in vivo* (Martins *et al.*, 2015). Notably, BRI1 and ERECTA do not share the same E3-ligases, as BRI1 is ubiquitinated by PUB12/13, whereas ERECTA is ubiquitinated by PUB30/31 (Zhou *et al.*, 2018; Chen *et al.*, 2023). Nevertheless, the finding that ERECTA is polyubiquitinated by K63-linked but not by K48-linked ubiquitins (Fig. 3b) adds to growing evidence for the K63-linked poly-ubiquitination as a shared regulatory mechanism of plant receptor kinase endocytosis and subsequent receptor degradation (Saeed *et al.*, 2023). Interestingly, although K63-linked ubiquitination is diminished in the $ERECTA_{3KR}$ mutant (Fig. 3c), anti-HA immunoblot still shows a smear, suggesting that other forms of ubiquitination may still occur in the protoplast system. It is highly likely that these PUB-type E3 ligases pair up with E2 ubiquitin-conjugating enzymes (e.g. UBC35/UBC36) to mediate K63-linked ubiquitination (Saeed *et al.*, 2023). In addition to BRI1, the turnover of the immune receptor FLS2 requires UBC35/UBC36; although these E2s can assemble K63-linked chains, the precise polyubiquitin linkage chain types on FLS2 itself remain unclear (Saeed *et al.*, 2023; Hasegawa *et al.*, 2024). However, *ubc35 ubc36* double mutant plants exhibit no discernible phenotypes in stomatal or pedicel development (Fig. S5), suggesting that these E2 enzymes have a less direct impact on the resulting phenotype than the corresponding E3 ligases, PUB30 and PUB31. This lack of obvious phenotype may be attributed to the pleiotropic nature of E2 enzymes, functional redundancy within the E2 enzymes, or potential competition among various E3 ligases for the same E2 partners.

It is important to note that the developmental role of ERECTA imposes stricter spatial constraints. ERECTA interprets multiple EPF/EPFL peptides to control stomatal patterning, a process that requires signaling to be confined both spatially and temporally, often at the level of individual cell files (Torii, 2012; Tameshige *et al.*, 2017). Our study shows that PUB30/PUB31-mediated attenuation of ERECTA via ubiquitination, receptor internalization, and vacuolar degradation is essential for maintaining positional fidelity and preventing ectopic signal activation (Figs 4, 5). By contrast, FLS2 responds to broadly diffusible pathogen-associated signals to trigger acute immune responses (Chinchilla *et al.*, 2007). Although BRI1 signaling shows tissue-specific outputs depending on developmental context (Planas-Riverola *et al.*, 2019; Blanco-Touriñán *et al.*, 2024), its endocytosis has been studied using seedling roots, where BRI1 is uniformly expressed (Di Rubbo *et al.*, 2013; Zhou *et al.*, 2018; Saeed *et al.*, 2023). It has become evident that tissue- and cell-type-specific regulation of signaling events is critical for immunity and development (Sparks *et al.*, 2013; Fukuda & Hardtke, 2019; Han & Tsuda, 2023). As such, the knowledge obtained through this study will help unravel how receptor trafficking defines positional information in plants.

There has been a debate over whether plant receptors signal exclusively at the plasma membrane or if their signaling activity is sustained in endosomes after the ligand-induced internalization, similar to what is observed for the EPIDERMAL GROWTH FACTOR (EGF) receptor kinases in mammals (Lai *et al.*, 1989; Pinilla-Macua *et al.*, 2025). In the case of BRI1, early evidence

© 2026 The Author(s).
New Phytologist © 2026 New Phytologist Foundation.

suggested its endosomal signaling (Geldner *et al.*, 2007). A subsequent study presented that increasing BRI1 population in the TGN/EE did not affect BR signaling, thus suggesting that BRI1 signals from the plasma membrane (Irani *et al.*, 2012; Zhang *et al.*, 2019). Our study shows that the K63-ubiquitination-deficient mutant of ERECTA ($ERECTA_{3KR}$) stably accumulates at the plasma membrane and severely compromises ligand-induced endocytosis (Fig. 4). Importantly, this severe reduction of ERECTA endocytosis results in hyperactivity of ERECTA signaling, leading to over-inhibition of stomatal development as well as excessive elongation of pedicels (Figs 1, 2, S1). Taken together, our work provides evidence supporting that ERECTA signals at the plasma membrane.

Several key questions remain unresolved. How ERECTA ubiquitination interfaces with broader endomembrane processes (Banjade *et al.*, 2019), as well as how distinct EPF/EPFL peptide ligands and co-receptors (e.g. TMM, BAK1/SERKS: Fig. 6) influence the dynamics of ERECTA endocytosis, remains to be clarified. Likewise, how ERECTA ubiquitination cooperates with or antagonizes other post-translational modifications, such as phosphorylation, to form combinatorial regulatory outputs is an important area for future investigation (Zhang & Zeng, 2020). Moreover, it has not been established whether environmental or hormonal cues modulate ERECTA ubiquitination, thereby linking external signals to the spatial control of stomatal development (Qi & Torii, 2018). Finally, the K63-linked ubiquitination attenuates multiple receptor kinases, including ERECTA, BRI1, and FLS2, pointing to a conserved mechanism that limits receptor longevity in contexts requiring tight signaling control (Saeed *et al.*, 2023). Comparative analyses across species and RLK subclasses may uncover shared principles underlying membrane receptor regulation in plants. Together, these questions point toward a broader framework for understanding how signaling precision is achieved through layered post-translational control of receptor homeostasis.

Acknowledgements

We thank Prof. Takashi Ueda and Prof. Kazuo Ebine for a gift of ARA6-RFP and SYP43-RFP marker lines and insightful suggestions and discussion about receptor endocytosis, and Prof. Marco Trujillo and Prof. Libo Shan for a gift of UBC35 and UBC8 plasmids, respectively. We appreciate the Torii Lab members, especially Dr Krishna Sepuru, for the discussion. This work was supported by funding from the Howard Hughes Medical Institute and the start-up fund from The University of Texas at Austin, as well as the Johnson & Johnson Centennial Chair awarded to K.U.T.

Competing interests

None declared.

Author contributions

LC and KUT conceptualized the research. LC, MHV, PB and KUT designed the research. LC, MHV, PB, AMC, CFY and KUT performed the experiments (LC, MHV and PB performed the biochemistry experiments; LC and MHV performed the confocal microscopy). LC, MHV, PB and KUT analyzed the data and performed the visualization. LC and KUT wrote the original manuscript. LC, MHV, AMC, CFY and KUT edited the manuscript. KUT acquired the funding. The final manuscript has been read and approved by all authors. LC and MHV contributed equally to this work.

ORCID

Pengfei Bai https://orcid.org/0000-0002-2281-2881
Liangliang Chen https://orcid.org/0000-0001-5740-7221
Keiko U. Torii https://orcid.org/0000-0002-6168-427X
Minh Huy Vu https://orcid.org/0000-0002-1963-2759
Crystal F. Ying https://orcid.org/0009-0007-8318-9142

Data availability

Supporting data for all results of this study are provided in Figs S1–S5, Tables S1 and S2 of Supporting Information, and Dataset S1. The accession numbers are as follows: *Arabidopsis thaliana* AtERL1 (AT5G62230.1), AtERL2 (AT5G07180.1), AtERECTA (AT2G26330.1), *Arabidopsis lyrata* AlERECTA (XP_020884443.1), *Capsella rubella* CrERECTA (XP_006296065.1), *Brassica napus* (AGL91677.1), *Eutrema salsugineum* (Pall.) EsERECTA (XP_006408746.1), *Glycine soja* GsERECTA (KHN37058.1), *Solanum lycospersicum* SlERECTA (XP_004245043.1), *Populus trichocarpa* PtERECTA (XP_024458576.1), *Oryza sativa cv japonica* OsERECTA (XP_015642019.1), *Brachypodium distachyon* BdERECTA (KQK19116.1), *Marchantia polymorpha* MpERECTA (Mapoly0070s0019.1), and *Physcomitrella patens* PpERECTA1 (Pp3c2_22410V3.1), PpERECTA2 (Pp3c1_17360V3.1), and PpERECTA3 (Pp3c21_9500V3.1). The materials generated and used in this study are available from the corresponding author upon reasonable request.

References

Abrash EB, Bergmann DC. 2010. Regional specification of stomatal production by the putative ligand CHALLAH. *Development* **137**: 447–455.

Aniento F, Sánchez de Medina Hernández V, Dagdas Y, Rojas-Pierce M, Russinova E. 2021. Molecular mechanisms of endomembrane trafficking in plants. *Plant Cell* **34**: 146–173.

Bai P, Torii KU. 2026. ERECTA-family receptor kinases: versatile regulators of developmental signaling. *The Plant Journal* **125**: e70793.

Banjade S, Tang S, Shah YH, Emr SD. 2019. Electrostatic lateral interactions drive ESCRT-III heteropolymer assembly. *eLife* **8**: e46207.

Blanco-Touriñán N, Rana S, Nolan TM, Li K, Vukašinović N, Hsu C-W, Russinova E, Hardtke CS. 2024. The brassinosteroid receptor gene BRI1 safeguards cell-autonomous brassinosteroid signaling across tissues. *Science Advances* **10**: eadq3352.

Chen L, Cochran AM, Waite JM, Shirasu K, Bemis SM, Torii KU. 2023. Direct attenuation of Arabidopsis ERECTA signalling by a pair of U-box E3 ligases. *Nature Plants* **9**: 112–127.

Chen L, Maes M, Cochran AM, Avila JR, Derbyshire P, Sklenar J, Haas KM, Villén J, Menke FLH, Torii KU. 2025. Preventing inappropriate signals pre- and post-ligand perception by a toggle switch mechanism of ERECTA. *Proceedings of the National Academy of Sciences, USA* **122**: e2420196122.

© 2026 The Author(s).
New Phytologist © 2026 New Phytologist Foundation.

Chinchilla D, Zipfel C, Robatzek S, Kemmerling B, Nürnberger T, Jones JDG, Felix G, Boller T. 2007. A flagellin-induced complex of the receptor FLS2 and BAK1 initiates plant defence. *Nature* **448**: 497–500.

Dejonghe W, Kuenen S, Mylle E, Vasileva M, Keech O, Viotti C, Swerts J, Fendrych M, Ortiz-Morea FA, Mishev K *et al.* 2016. Mitochondrial uncouplers inhibit clathrin-mediated endocytosis largely through cytoplasmic acidification. *Nature Communications* **7**: 11710.

Di Rubbo S, Irani NG, Kim SY, Xu Z-Y, Gadeyne A, Dejonghe W, Vanhoutte I, Persiau G, Eeckhout D, Simon S *et al.* 2013. The clathrin adaptor complex AP-2 mediates endocytosis of BRASSINOSTEROID INSENSITIVE1 in Arabidopsis. *Plant Cell* **25**: 2986–2997.

Dubeaux G, Neveu J, Zelazny E, Vert G. 2018. Metal sensing by the IRT1 transporter-receptor orchestrates its own degradation and plant metal nutrition. *Molecular Cell* **69**: 953–964.

Ebine K, Fujimoto M, Okatani Y, Nishiyama T, Goh T, Ito E, Dainobu T, Nishitani A, Uemura T, Sato MH *et al.* 2011. A membrane trafficking pathway regulated by the plant-specific RAB GTPase ARA6. *Nature Cell Biology* **13**: 853–859.

Foissner I, Sommer A, Hoeftberger M, Hoepflinger MC, Absolonova M. 2016. Is Wortmannin-induced reorganization of the *trans*-golgi network the key to explain charasome formation? *Frontiers in Plant Science* **7**: 756.

Foot N, Henshall T, Kumar S. 2017. Ubiquitination and the regulation of membrane proteins. *Physiological Reviews* **97**: 253–281.

Fukuda H, Hardtke CS. 2019. Peptide signaling pathways in vascular differentiation. *Plant Physiology* **182**: 1636–1644.

Geldner N, Hyman DL, Wang X, Schumacher K, Chory J. 2007. Endosomal signaling of plant steroid receptor kinase BRI1. *Genes & Development* **21**: 1598–1602.

Grubb LE, Derbyshire P, Dunning KE, Zipfel C, Menke FLH, Monaghan J. 2021. Large-scale identification of ubiquitination sites on membrane-associated proteins in *Arabidopsis thaliana* seedlings. *Plant Physiology* **185**: 1483–1488.

Han X, Tsuda K. 2023. Divide and conquer: spatiotemporal plant innate immunity at single-cell resolution. *Cell Host & Microbe* **31**: 1601–1603.

Hara K, Kajita R, Torii KU, Bergmann DC, Kakimoto T. 2007. The secretory peptide gene EPF1 enforces the stomatal one-cell-spacing rule. *Genes & Development* **21**: 1720–1725.

Hara K, Yokoo T, Kajita R, Onishi T, Yahata S, Peterson KM, Torii KU, Kakimoto T. 2009. Epidermal cell density is autoregulated via a secretory peptide, EPIDERMAL PATTERNING FACTOR 2 in Arabidopsis leaves. *Plant & Cell Physiology* **50**: 1019–1031.

Hasegawa Y, Luo Y, Sato T. 2024. Recent advances in ubiquitin signals regulating plant membrane trafficking. *Plant & Cell Physiology* **65**: 1907–1924.

Horst RJ, Fujita H, Lee JS, Rychel AL, Garrick JM, Kawaguchi M, Peterson KM, Torii KU. 2015. Molecular framework of a regulatory circuit initiating two-dimensional spatial patterning of stomatal lineage. *PLoS Genetics* **11**: e1005374.

Hunt L, Gray JE. 2009. The signaling peptide EPF2 controls asymmetric cell divisions during stomatal development. *Current Biology* **19**: 864–869.

Irani NG, Di Rubbo S, Mylle E, Van den Begin J, Schneider-Pizoń J, Hniliková J, Šíša M, Buyst D, Vilarrasa-Blasi J, Szatmári A-M *et al.* 2012. Fluorescent castasterone reveals BRI1 signaling from the plasma membrane. *Nature Chemical Biology* **8**: 583–589.

Kleine-Vehn J, Łangowski Ł, Wiśniewska J, Dhonukshe P, Brewer PB, Friml J. 2008. Cellular and molecular requirements for polar PIN targeting and transcytosis in plants. *Molecular Plant* **1**: 1056–1066.

Kondo T, Kajita R, Miyazaki A, Hokoyama M, Nakamura-Miura T, Mizuno S, Masuda Y, Irie K, Tanaka Y, Takada S *et al.* 2010. Stomatal density is controlled by a mesophyll-derived signaling molecule. *Plant & Cell Physiology* **51**: 1–8.

Kraft E, Stone SL, Ma L, Su N, Gao Y, Lau OS, Deng XW, Callis J. 2005. Genome analysis and functional characterization of the E2 and RING-type E3 ligase ubiquitination enzymes of Arabidopsis. *Plant Physiology* **139**: 1597–1611.

Lai WH, Cameron PH, Doherty JJ 2nd, Posner BI, Bergeron JJ. 1989. Ligand-mediated autophosphorylation activity of the epidermal growth factor receptor during internalization. *Journal of Cell Biology* **109**: 2751–2760.

Lampard GR, MacAlister CA, Bergmann DC. 2008. Arabidopsis stomatal initiation is controlled by MAPK-mediated regulation of the bHLH SPEECHLESS. *Science* **322**: 1113–1116.

Lee JS, Hnilova M, Maes M, Lin YC, Putarjunan A, Han SK, Avila J, Torii KU. 2015. Competitive binding of antagonistic peptides fine-tunes stomatal patterning. *Nature* **522**: 439–443.

Lee JS, Kuroha T, Hnilova M, Khatayevich D, Kanaoka MM, McAbee JM, Sarikaya M, Tamerler C, Torii KU. 2012. Direct interaction of ligand–receptor pairs specifying stomatal patterning. *Genes & Development* **26**: 126–136.

Leitner J, Petrášek J, Tomanov K, Retzer K, Pařezová M, Korbei B, Bachmair A, Zažímalová E, Luschnig C. 2012. Lysine63-linked ubiquitylation of PIN2 auxin carrier protein governs hormonally controlled adaptation of Arabidopsis root growth. *Proceedings of the National Academy of Sciences, USA* **109**: 8322–8327.

Lin G, Zhang L, Han Z, Yang X, Liu W, Li E, Chang J, Qi Y, Shpak ED, Chai J. 2017. A receptor-like protein acts as a specificity switch for the regulation of stomatal development. *Genes & Development* **31**: 927–938.

Lu D, Lin W, Gao X, Wu S, Cheng C, Avila J, Heese A, Devarenne TP, He P, Shan L. 2011. Direct ubiquitination of pattern recognition receptor FLS2 attenuates plant innate immunity. *Science* **332**: 1439–1442.

Martins S, Dohmann EMN, Cayrel A, Johnson A, Fischer W, Pojer F, Satiat-Jeunemaître B, Jaillais Y, Chory J, Geldner N *et al.* 2015. Internalization and vacuolar targeting of the brassinosteroid hormone receptor BRI1 are regulated by ubiquitination. *Nature Communications* **6**: 6151.

Meckel T, Hurst AC, Thiel G, Homann U. 2004. Endocytosis against high turgor: intact guard cells of *Vicia faba* constitutively endocytose fluorescently labelled plasma membrane and GFP-tagged K^+-channel KAT1. *The Plant Journal* **39**: 182–193.

Meng X, Chen X, Mang H, Liu C, Yu X, Gao X, Torii KU, He P, Shan L. 2015. Differential function of Arabidopsis SERK family receptor-like kinases in stomatal patterning. *Current Biology* **25**: 2361–2372.

Meng X, Wang H, He Y, Liu Y, Walker JC, Torii KU, Zhang S. 2012. A MAPK cascade downstream of ERECTA receptor-like protein kinase regulates Arabidopsis inflorescence architecture by promoting localized cell proliferation. *Plant Cell* **24**: 4948–4960.

Nadeau JA, Sack FD. 2002. Control of stomatal distribution on the Arabidopsis leaf surface. *Science* **296**: 1697–1700.

Pillitteri LJ, Peterson KM, Horst RJ, Torii KU. 2011. Molecular profiling of stomatal meristemoids reveals new component of asymmetric cell division and commonalities among stem cell populations in Arabidopsis. *Plant Cell* **23**: 3260–3275.

Pillitteri LJ, Torii KU. 2012. Mechanisms of stomatal development. *Annual Review of Plant Biology* **63**: 591–614.

Pinilla-Macua I, Surve S, Sorkin A. 2025. Cell migration signaling through the EGFR-VAV2-Rac1 pathway is sustained in endosomes. *Journal of Cell Science* **138**: jcs263541.

Planas-Riverola A, Gupta A, Betegón-Putze I, Bosch N, Ibañes M, Caño-Delgado AI. 2019. Brassinosteroid signaling in plant development and adaptation to stress. *Development* **146**: dev151894.

Postma J, Liebrand TWH, Bi G, Evrard A, Bye RR, Mbengue M, Kuhn H, Joosten MHAJ, Robatzek S. 2016. Avr4 promotes Cf-4 receptor-like protein association with the BAK1/SERK3 receptor-like kinase to initiate receptor endocytosis and plant immunity. *New Phytologist* **210**: 627–642.

Qi X, Han SK, Dang JH, Garrick JM, Ito M, Hofstetter AK, Torii KU. 2017. Autocrine regulation of stomatal differentiation potential by EPF1 and ERECTA-LIKE1 ligand-receptor signaling. *eLife* **6**: e24102.

Qi X, Torii KU. 2018. Hormonal and environmental signals guiding stomatal development. *BMC Biology* **16**: 21.

Qi X, Yoshinari A, Bai P, Maes M, Zeng SM, Torii KU. 2020. The manifold actions of signaling peptides on subcellular dynamics of a receptor specify stomatal cell fate. *eLife* **9**: e58097.

Reyes FC, Buono R, Otegui MS. 2011. Plant endosomal trafficking pathways. *Current Opinion in Plant Biology* **14**: 666–673.

Romero-Barrios N, Vert G. 2018. Proteasome-independent functions of lysine-63 polyubiquitination in plants. *New Phytologist* **217**: 995–1011.

Saeed B, Deligne F, Brillada C, Dünser K, Ditengou FA, Turek I, Allahham A, Grujic N, Dagdas Y, Ott T *et al.* 2023. K63-linked ubiquitin chains are a global signal for endocytosis and contribute to selective autophagy in plants. *Current Biology* **33**: 1337–1345.

© 2026 The Author(s).
New Phytologist © 2026 New Phytologist Foundation.

Santuari L, Scacchi E, Rodriguez-Villalon A, Salinas P, Dohmann EMN, Brunoud G, Vernoux T, Smith RS, Hardtke CSE. 2011. Positional information by differential endocytosis splits auxin response to drive Arabidopsis root meristem growth. *Current Biology* **21**: 1918–1923.

Shpak ED. 2013. Diverse roles of ERECTA family genes in plant development. *Journal of Integrative Plant Biology* **55**: 1238–1250.

Shpak ED, Berthiaume CT, Hill EJ, Torii KU. 2004. Synergistic interaction of three ERECTA-family receptor-like kinases controls Arabidopsis organ growth and flower development by promoting cell proliferation. *Development* **131**: 1491–1501.

Shpak ED, Lakeman MB, Torii KU. 2003. Dominant-negative receptor uncovers redundancy in the Arabidopsis ERECTA leucine-rich repeat receptor-like kinase signaling pathway that regulates organ shape. *Plant Cell* **15**: 1095–1110.

Shpak ED, McAbee JM, Pillitteri LJ, Torii KU. 2005. Stomatal patterning and differentiation by synergistic interactions of receptor kinases. *Science* **309**: 290–293.

Sparks E, Wachsman G, Benfey PN. 2013. Spatiotemporal signalling in plant development. *Nature Reviews Genetics* **14**: 631–644.

Sugano SS, Shimada T, Imai Y, Okawa K, Tamai A, Mori M, Hara-Nishimura I. 2010. Stomagen positively regulates stomatal density in Arabidopsis. *Nature* **463**: 241–244.

Tameshige T, Ikematsu S, Torii KU, Uchida N. 2017. Stem development through vascular tissues: EPFL–ERECTA family signaling that bounces in and out of phloem. *Journal of Experimental Botany* **68**: 45–53.

Torii KU. 2012. Mix-and-match: ligand–receptor pairs in stomatal development and beyond. *Trends in Plant Science* **17**: 711–719.

Torii KU, Mitsukawa N, Oosumi T, Matsuura Y, Yokoyama R, Whittier RF, Komeda Y. 1996. The Arabidopsis ERECTA gene encodes a putative receptor protein kinase with extracellular leucine-rich repeats. *Plant Cell* **8**: 735–746.

Trujillo M. 2021. Ubiquitin signalling: controlling the message of surface immune receptors. *New Phytologist* **231**: 47–53.

Turek I, Tischer N, Lassig R, Trujillo M. 2018. Multi-tiered pairing selectivity between E2 ubiquitin–conjugating enzymes and E3 ligases. *Journal of Biological Chemistry* **293**: 16324–16336.

Uchida N, Lee JS, Horst RJ, Lai H-H, Kajita R, Kakimoto T, Tasaka M, Torii KU. 2012. Regulation of inflorescence architecture by intertissue layer ligand-receptor communication between endodermis and phloem. *Proceedings of the National Academy of Sciences, USA* **109**: 6337–6342.

Wang D, Yang C, Wang H, Wu Z, Jiang J, Liu J, He Z, Chang F, Ma H, Wang X. 2017. BKI1 regulates plant architecture through coordinated inhibition of the brassinosteroid and ERECTA signaling pathways in Arabidopsis. *Molecular Plant* **10**: 297–308.

Wang J, Cai Y, Miao Y, Lam SK, Jiang L. 2009. Wortmannin induces homotypic fusion of plant prevacuolar compartments. *Journal of Experimental Botany* **60**: 3075–3083.

Zhang L, Liu Y, Zhu XF, Jung JH, Sun Q, Li TY, Chen LJ, Duan YX, Xuan YH. 2019. SYP22 and VAMP727 regulate BRI1 plasma membrane targeting to control plant growth in Arabidopsis. *New Phytologist* **223**: 1059–1065.

Zhang Y, Zeng L. 2020. Crosstalk between ubiquitination and other post-translational protein modifications in plant immunity. *Plant Communications* **1**: 100041.

Zhou J, Liu D, Wang P, Ma X, Lin W, Chen S, Mishev K, Lu D, Kumar R, Vanhoutte I *et al.* 2018. Regulation of Arabidopsis brassinosteroid receptor BRI1 endocytosis and degradation by plant U-box PUB12/PUB13-mediated ubiquitination. *Proceedings of the National Academy of Sciences, USA* **115**: E1906–E1915.

Supporting Information

Additional Supporting Information may be found online in the Supporting Information section at the end of the article.

Dataset S1 Source data for Figs 1–5 and Figs S1–S5.

Fig. S1 Ubiquitination-deficient ERECTA overly promotes pedicel growth, related to Fig. 2.

Fig. S2 Expression level of *ERECTA* in *ERECTA-FLAG er*, *ERECTA$_{3KR}$-FLAG er*, *ERECTA-YFP er*, *ERECTA$_{3KR}$-YFP er*, related to Fig. 2.

Fig. S3 The predicted ubiquitination sites are required for polyubiquitination of ERECTA by PUB31, related to Fig. 3.

Fig. S4 K63-linked ubiquitination is required for eventual vacuolar degradation of ERECTA, related to Fig. 5.

Fig. S5 The *ubc35 ubc36* double mutant exhibits normal stomatal development and pedicel elongation.

Table S1 List of plasmids used in this study.

Table S2 List of primers used in this study.

Please note: Wiley is not responsible for the content or functionality of any Supporting Information supplied by the authors. Any queries (other than missing material) should be directed to the *New Phytologist* Central Office.

Disclaimer: The New Phytologist Foundation remains neutral with regard to jurisdictional claims in maps and in any institutional affiliations.

© 2026 The Author(s).
New Phytologist © 2026 New Phytologist Foundation.